

# Closed Loop Reference Optimization for Extrusion Additive Manufacturing

Rawan Hoteit <sup>\*</sup>, Andrea Balestra <sup>\*\*</sup>, Nathan Mingard <sup>\*\*</sup>,  
Efe C. Balta <sup>\*,\*\*</sup>, John Lygeros <sup>\*</sup>

<sup>\*</sup> Department of Information Technology and Electrical Engineering at ETH Zürich, Switzerland (e-mail: [{rhoteit, jlygeros}@ethz.ch](mailto:{rhoteit, jlygeros}@ethz.ch))

<sup>\*\*</sup> inspire AG, Zürich, Switzerland (e-mail: [{andrea.balestra, nathan.mingard, efe.balta}@inspire.ch](mailto:{andrea.balestra, nathan.mingard, efe.balta}@inspire.ch))

**Abstract:** Various defects occur during material extrusion additive manufacturing processes that degrade the quality of the 3D printed parts and lead to significant material waste. This motivates feedback control of the extrusion process to mitigate defects and prevent print failure. We propose a linear quadratic regulator (LQR) for closed-loop control with force feedback to provide accurate width tracking of the extruded filament. Furthermore, we propose preemptive optimization of the reference force given to the LQR that accounts for the performance of the LQR and generates the optimal reference for the closed loop extrusion dynamics and machine constraints. Simulation results demonstrate the improved tracking performance and response time. Experiments on a Fused Filament Fabrication 3D printer showcase a root mean square error improvement of 39.57% compared to tracking the unmodified reference as well as an 83.7% shorter settling time.

**Keywords:** Additive manufacturing, intelligent manufacturing systems, advanced process control, control of complex systems, parametric optimization, control and optimization

## 1. INTRODUCTION

Additive manufacturing (AM), or 3D printing, has recently gained considerable traction in a range of industries, from aerospace and automotive engineering to biomedical applications. One such process is Fused Filament Fabrication (FFF), in which plastic is melted and extruded from an extrusion head that is attached to a 3-axis gantry system (Singh et al. (2020)). Various disturbances that occur during the AM process compromise the quality of the print, due to over- and under-extrusion. Extrusion errors result in unintended accumulation or lack of filament at a specific print location in the layer. Moreover, extrusion errors generally lead to considerable post-processing or complete part failure, resulting in significant material waste.

Over-extrusion is often evident around corners where the extrusion head slows down, causing an accumulation of material at that location. This necessitates modeling the extrusion dynamics (Bellini et al. (2004)) to predict and prevent such defects. Exploiting the interplay between the motion and extrusion dynamics, Kuipers et al. (2020) generate contour-parallel tool-paths with varying widths via back-pressure compensation. Zhang et al. (2024) use flow front boundary equations to model the resulting extrusion height and width, while Balta and Altinkaynak (2022) characterize the cross-sectional geometry of deposited ma-

terial in extrusion AM using numerical models. A simplified linear extrusion model is used by Chesser et al. (2019) to design a feedforward controller that minimizes the tradeoff between printing speed and printing resolution. Moreover, Wu et al. (2021) design a feedforward controller based on nonlinear extrusion dynamics to inhibit over- and under-extrusion defects, and present a framework to coordinate motion and extrusion to operate in a region that validates the simplified linear extrusion model. Subsequent work by Wu et al. (2023) considers discontinuous extrusion flow rate due to the retraction effects on the filament. Gao et al. (2025) design and validate a nonlinear lead-based feedforward controller after modeling the varying time constant associated with the extrusion model for different printing speeds. Furthermore, a feedforward iterative learning controller is implemented by Bahrami et al. (2025) for direct ink writing while modeling the interplay between the extrusion and motion dynamics, using vision-based width estimates.

Most of the schemes above rely on feedforward control to compensate for over- and under-extrusion. Feedforward control suffers from open-loop limitations and cannot compensate for sudden defects during printing. Thus, reducing these effects requires in-process monitoring, control and optimization. In similar AM processes, in-process control is proposed by Shi et al. (2018) using a PI controller for laser metal deposition printing. Moreover, Rabiei and Moini (2025) design a PID to control the extrusion rate for concrete AM using the extrusion pressure measured using a load cell. A model predictive controller, is approximated

<sup>\*</sup> Research supported by the NCCR Automation, a National Centre of Competence in Research, funded by the Swiss National Science Foundation (grant number 51NF40-225155) and by the BRIDGE Discovery programme of the Swiss National Science Foundation and Innosuisse (grant number 226437).

by a neural network by Zomorodi and Landers (2016) for various ceramic printing modes.

According to Moretti et al. (2021), in-process monitoring and feedback are considered essential in FFF to inhibit extrusion defects or correct them if they were to occur. Fravolini et al. (2025) compute the optimal extrusion feed rate via a Quadratic Programming (QP) formulation that is constrained on linear extrusion dynamics and system constraints. Additionally, Moretti and Rossi (2023) design a PID-based filament transport controller into the printing extruder, while Hornus et al. (2020) determine varying extrusion width-based paths to minimize extrusion error. Incorporating the linearized dynamics and constraints of the extruder into a model predictive controller is proposed by Xia et al. (2020) based on a vision-based system for extrusion width measurement.

Recent work proposes an in-situ force measurement setup called Force Controlled Printing (FCP). First demonstrated with PID control, FCP is shown to achieve state of the art width control (Guidetti et al. (2024a)), and is used in parametric optimization of control parameters (Guidetti et al. (2024b)). This work explicitly establishes a relationship between the extrusion force and the resulting filament width on the print bed, and enables the closed-loop control of the geometry of the extruded filament.

Here we go beyond this state of the art and utilize a linear quadratic regulator (LQR) for extrusion control, based on the FCP setup. We wrap the lower level controller within an optimization scheme that can anticipate the shortcomings of the closed loop system in a formulation similar to the reference governor (Kolmanovsky et al. (2014)). Specifically, the contributions of the paper are as follows:

- The formulation of an optimization problem for reference generation for closed loop extrusion control in additive manufacturing;
- The consideration of sim-to-real gap and automatic generation of G-code based on spatiotemporal constraints of the physical system.

To validate the contributions, we implement the proposed algorithm in real-time on a hardware setup, achieving an enhancement of the tracking error and quicker response time. The design and implementation of such an architecture is novel for extrusion-based additive manufacturing applications.

The paper is organized as follows: Section 2 presents the dynamics and complete control architecture including the optimization formulation. Then, the simulation and experimental results can be seen in Section 3; finally, the paper is concluded in Section 4.

## 2. SYSTEM ARCHITECTURE

### 2.1 Dynamics

The extrusion head in FFF (Fig. 1) comprises a motor attached to two rollers that feed a polymer-based filament into a heated nozzle. The nozzle melts the filament to deposit a plastic bead. The extruder then moves in space and forms lines of specific widths onto a heated printing bed. Guidetti et al. (2024a) demonstrate that the relation-

ship between the reactive force experienced by the rollers and the line width is linear; this allows one to indirectly measure the line width by measuring the reactive force and inverting the linear relationship. The reaction force can be measured using the force sensor designed by Guidetti et al. (2024a), as illustrated in Fig. 1.

The extrusion dynamics of the 3D printer are assumed to

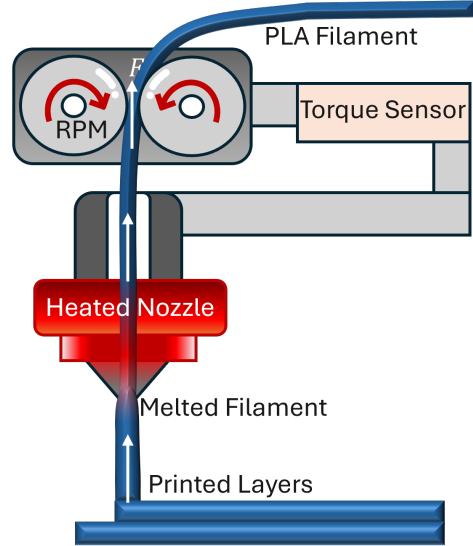


Fig. 1. Fused Filament Fabrication (FFF) Process  
follow a discrete time state space representation:

$$\begin{aligned} x_{k+1} &= Ax_k + Bu_k, \\ F_k &= Cx_k, \end{aligned} \quad (1)$$

where  $x_k \in \mathbb{R}^n$  is the system state obtained through system identification of the model linking the RPM to the measured force,  $u_k$  is the input corresponding to the motor RPM,  $F_k$  is the measured force and  $A$ ,  $B$  and  $C$  are the discrete time system matrices of appropriate dimensions. An LQR controller can be designed based on (1) to provide output-reference tracking. The input at time instance  $k$  is then given by:

$$u_k = -K_{LQR}(x_k - x_{ss,k}) + u_{ss,k}. \quad (2)$$

The steady state values of the state  $x_{ss,k}$  and of the input  $u_{ss,k}$  are computed as a function of the reference force  $r_F$  to be tracked:

$$\begin{bmatrix} I_n - A & -B \\ C & 0 \end{bmatrix} \begin{bmatrix} x_{ss,k} \\ u_{ss,k} \end{bmatrix} = \begin{bmatrix} \mathbb{0}_n \\ r_{F,k} \end{bmatrix} \quad (3)$$

where  $I_n$  is the identity matrix with dimensions  $n \times n$  and  $\mathbb{0}_n$  is the vector of all-zeroes in  $\mathbb{R}^n$ .  $K_{LQR} = (R + B^\top PB)^{-1}B^\top PA$  is the LQR gain computed using the solution of the discrete time Algebraic Riccati Equation:

$$P = A^\top PA - (A^\top PB)(R + B^\top PB)^{-1}(B^\top PA) + Q, \quad (4)$$

such that  $Q$  and  $R$  are the symmetric weight matrices associated with  $x_k$  and  $u_k$  in the LQR cost function:

$$J = \sum_{t=1}^T (x_t^\top Q x_t + u_t^\top R u_t). \quad (5)$$

### 2.2 Optimization Formulation

The translation from space into the time domain is a function of the dynamics and printing speed. The desired

width profile in space occurs at specific time instances based on the predicted motion and speed of the extrusion head. This allows for the generation of  $r_F$  as a function of the time step using the discrete sampling time. In this way we generate a sequence of  $N$  reference forces  $r_F$ . However, if we give these directly to the LQR controller to track, the resulting force will be different from the desired one. Though LQR may provide enhanced force tracking compared to PID controllers, it is still purely feedback based, and suffers from performance limitations due to the performance limitations of the closed loop system, including long settling times. To provide some preview to the LQR controller, a QP problem is formulated to obtain the optimal reference force given to the closed-loop system (Fig. 2).

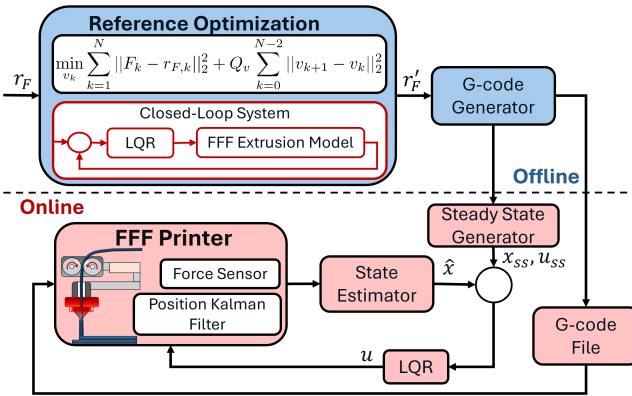


Fig. 2. Control Architecture

This is accomplished by solving the optimization problem:

$$\begin{aligned}
 & \min_{v_k} \sum_{k=1}^N \|F_k - r_{F,k}\|_2^2 + Q_v \sum_{k=0}^{N-2} \|v_{k+1} - v_k\|_2^2 \\
 & \text{s.t. } x_{k+1} = Ax_k + Bu_k \quad \forall k = 0, \dots, N-1 \\
 & \quad F_k = Cx_k \quad \forall k = 0, \dots, N \\
 & \quad \begin{bmatrix} I_n - A & -B \\ C & 0 \end{bmatrix} \begin{bmatrix} x_{ss,k} \\ u_{ss,k} \end{bmatrix} = \begin{bmatrix} 0_n \\ r_{F,k} + v_k \end{bmatrix} \\
 & \quad u_k = -K_{LQR}(x - x_{ss,k}) + u_{ss,k}, \quad \forall k = 0, \dots, N-1 \\
 & \quad u_k \in \mathcal{U} \quad \forall k = 0, \dots, N-1 \\
 & \quad r'_F \in \mathcal{R} \quad \forall k = 0, \dots, N-1 \\
 & \quad x_k \in \mathcal{X}. \quad \forall k = 0, \dots, N
 \end{aligned} \tag{6}$$

The input of the QP is a sequence of  $N$  reference forces, while the output is a modified sequence  $r'_F = r_F + v$  that is given to the LQR. The aim is that the resulting force  $F_k$  of the closed-loop system tracks the original desired reference  $r_F$  at time step  $k$ , compensating for the closed-loop performance of the extrusion system, while constraining the resulting force reference within thresholds set by the machine. In this work, we set the system limits to reflect the region where system identification was performed. The formulation also minimizes the variation of  $v_k$  to ensure smooth modified references between consecutive step sizes through an additional term in the objective function weighted by  $Q_v$ .

The optimal reference forces are found offline for the LQR to track in run-time.

### 2.3 G-code Generator

Applying the inputs computed for the discrete time model (1) directly to the system can cause real-time implementation issues, due to the communication delays in the G-code transmission. We account for this delay by imposing a zero-order hold on  $v_k$  over multiple time steps to obtain the optimal reference before generating the appropriate G-code. The number of steps in which  $v_k$  is held constant is denoted by the hold length  $N_h$ , which is lower-bounded by the execution frequency. This intrinsically translates into fixing a value of  $v$  for each  $j = 1, N_h, \dots, \lceil N/N_h \rceil$  or setting equality constraints in the optimization problem in (6):

$$v_k = c_j, \quad \forall k = 1, \dots, N, \quad j = 1, N_h, \dots, \lceil N/N_h \rceil \tag{7}$$

where  $c_j$  is a constant and  $\lceil \cdot \rceil$  is the ceiling function.

After solving the QP and obtaining  $r'_F$ , the G-code is generated using the motion-based mapping between space and time. The steady state values given to the LQR are then recomputed online as  $r'_F$  changes. Thus, this methodology considers the sim-to-real gap in terms of the communication pipeline and optimizes for the approximate discretized solution offline, making it executable on a real system.

## 3. TESTING AND VALIDATION

### 3.1 System Identification

The FFF extrusion head is attached to a 5-axis gantry which can move along 3 axes ( $x, y, z$ ) and the printing head can rotate along two axes; however, we constrain the motion along those two axes and solely implement planar printing throughout this paper. The printing bed, extrusion head/nozzle and corresponding force sensor can also be seen in Fig. 3. Note that the force value -as given from the sensor- has an inherent negative value.

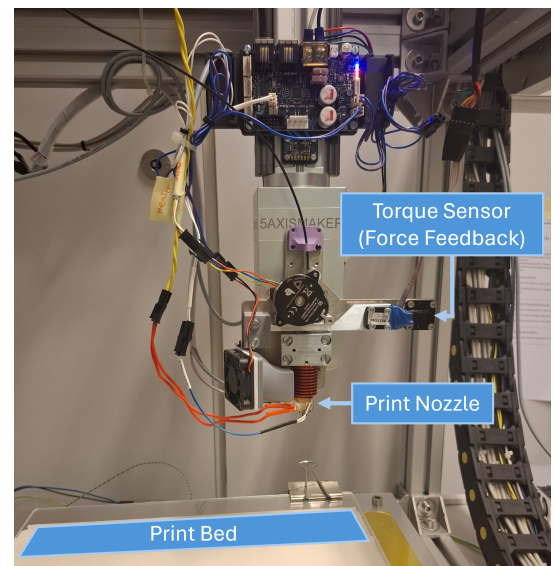


Fig. 3. Experimental Setup

By performing experiments on the system described in Section 2.1 and seen in Fig. 3, data was collected to identify

the extrusion system dynamics (1). Fixing  $\tau_s = 0.01$ s,  $n = 3$  and using the N4SID method by Van Overschee and De Moor (1994) gave rise to the matrices:

$$A = \begin{bmatrix} 1.00603451 & 0.01305934 & 0.0357625 \\ 0.00625487 & 1.01087517 & 0.0192488 \\ -0.33079381 & -0.7101034 & 0.5566053 \end{bmatrix},$$

$$B = \begin{bmatrix} 0.00008626 \\ -0.00008873 \\ 0.0047217 \end{bmatrix},$$

$$C = [-27.8759035 \ 0.22352502 \ -0.04037422].$$

Fixing

$$Q = \begin{bmatrix} 1656.2 & 0.0 & 0.0 \\ 0.0 & 8.9 & 0.0 \\ 0.0 & 0.0 & 1.6 \end{bmatrix}, \quad R = 0.00995, \quad (8)$$

then gave rise to the LQR controller with corresponding gain  $K_{LQR} = [323.8591 \ -113.4687 \ 23.2255]$ .

### 3.2 Validation in Simulation

In the first test, the reference force to be tracked by the LQR is given by a step function and optimized for over the full horizon via (6) (Fig. 4). The resulting force is shown in the second plot of Fig. 4, having better tracking of  $r_F$  in comparison to the original force without optimizing the reference ( $F_0$ ). The new reference  $r'_F$  is specifically modified near the time steps when the step occurs, for which the resulting extrusion force is  $F_{QP}$ . This is to account for the predicted behavior of the closed-loop system which has a large settling time whilst tracking the original reference. To quantify the improvement, consider the root mean squared error (RMSE)

$$RMSE(F, r_F) = \sqrt{\frac{1}{N} \sum_{k=1}^N (F_k - r_{F,k})^2}, \quad (9)$$

and the 5% settling time of the response  $t_{5\%}$ , defined as the time taken by the system to reach and remain within 5% of the final desired reference value. Commanding the extrusion system to track  $r'_F$  leads to an RSME of 0.0637N that is 69.8% smaller than the RSME of 0.211N obtained when commanding the system to track  $r_F$ . Correspondingly,  $t_{5\%}$  decreases from 0.185s when commanding the extrusion system to track  $r_F$  to 0.035s when commanding the system to track  $r'_F$ , a reduction of 81.08%. The corresponding RPM input is shown in Fig. 4. The input,  $u_{QP}$ , needed to track  $r'_F$  is significantly larger and is applied earlier than the input for  $r_F$ ,  $u_0$ . This is due to the preview provided by the QP that compensates for the slow response of the system.

To analyze the impact of various discretizations on the reference optimization, we consider  $v_k$  having a hold length  $N_h$  of 2 in  $v_{2,k}$ , and  $N_h = 5$  in  $v_{5,k}$ . The resulting output for a step function from  $-3N$  to  $-5N$  for the different discretizations can be seen in Fig. 5 and the resulting forces are presented in Fig. 5; a summary of the results can be found in Table 1.  $F_{QP,5}$ , the force corresponding to  $v_{5,k}$  and  $F_{QP,2}$  (resulting from applying  $v_{2,k}$ ) also lead to performance improvements in terms of RMSE and settling time. Compared to applying  $r_F$ , albeit larger than the one obtained with  $N_h = 1$ , having  $N_h = 2$  or  $N_h = 5$  leads to a RMSE that is 7.06% or 32.81% respectively

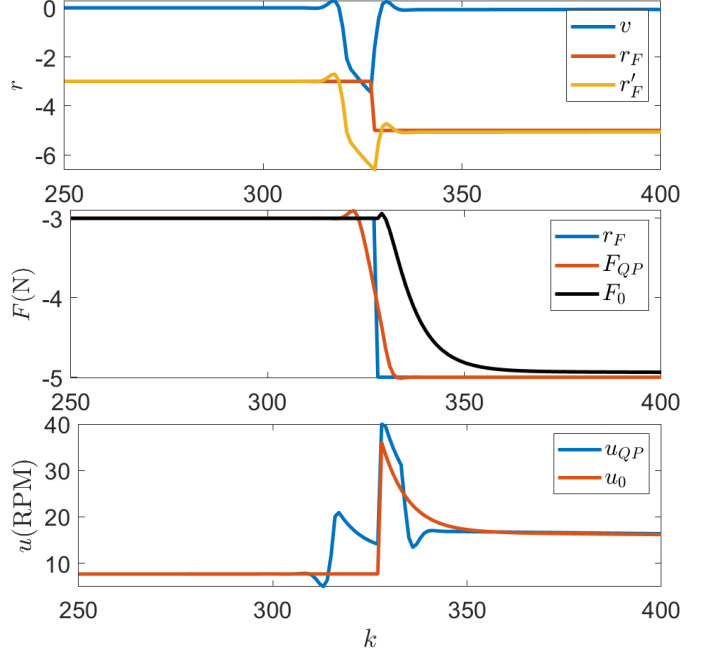


Fig. 4. Optimization of Step Reference in Simulation - Top: Original and Optimized Reference - Middle: Simulated Force - Bottom: Extrusion RPM Input

larger than that for  $F_{QP}$ . Increasing the hold length also leads to slightly higher settling time in comparison to the original resulting QP. However, we emphasize that the advantages of applying a zero-order hold are not apparent in simulation, but come into play in the experimental validation.

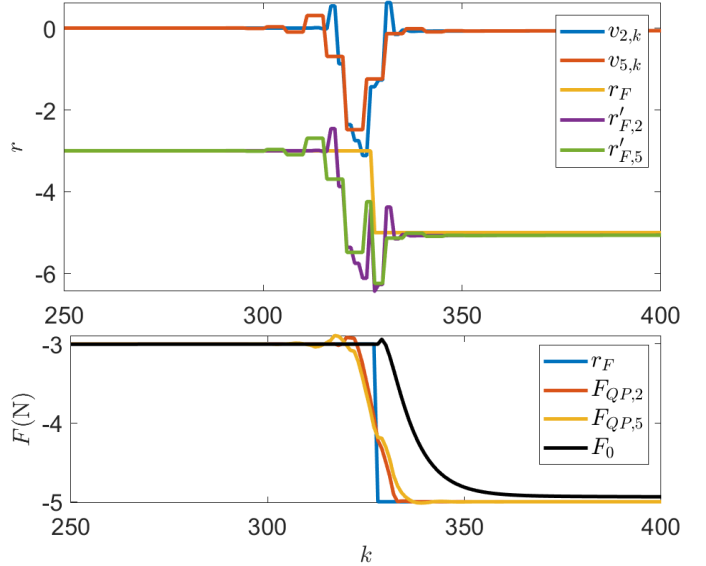


Fig. 5. Optimization of Step Reference in Simulation with  $N_h = \{2, 5\}$  - Top: Original and Discretized Optimal Force Reference - Bottom: Extrusion Force for Different Discretization Lengths

Metric	$r_F$	$N_h = 1$	$N_h = 2$	$N_h = 5$
RMSE (N)	0.211	0.0637	0.0682	0.0846
$t_{5\%}$ (s)	0.185	0.035	0.045	0.055

Table 1. Simulation Performance Comparison

### 3.3 Validation in Experiments

The experimental validation is implemented on the setup seen in Fig. 3. A Kalman filter is employed to estimate the position of the extrusion head; this is important for the synchronization of the force command with the corresponding desired position of the extrusion head along the printing bed. The synchronization between motion and extrusion is implemented via G-code commands given to the 3D printer for trajectory tracking and extrusion control based on the printing speed of the extrusion head. The system is run using a custom ROS2 interface that implements the state estimators for real time operation, and a Duet controller board that controls the motion and heating. The ROS2 system is also responsible for the computation of the  $x_{ss,k}$  and  $u_{ss,k}$ , as well as parsing the G-code.

The step response in Fig. 4 for which the  $r_F$  increases in value from 3N to 5N (given by a step from  $-3N$  to  $-5N$ ) is tested with  $N_h = 2$  and  $N_h = 5$ ; the corresponding optimal references  $r'_{F,2}$  and  $r'_{F,5}$  can be seen in Fig. 6 with the respective performance of the extrusion force. The input RPM applied on the filament is presented in Fig. 6 showcasing a similar trend to that in Fig. 4 with  $u_{QP}$  acting prior to the step time and having a higher value than that of  $u_0$ . This leads to enhanced performance in comparison to the case without reference optimization. Though the performance significantly improves, the difference in results between the simulations and experimental validation are due to the model mismatch in the simplifications of the extrusion dynamics during the system identification process.

A rheological-based analysis of the filament dynamics through the extrusion head reveals its nonlinearity with respect to the extrusion force (Bellini et al. (2004)). However, the linearization is necessary to design the LQR controller for real-time feedback and control actions during the print. Linearization leads to a tractable optimization problem when optimizing the reference off-line.

The improved response time can also be seen in the resulting print shown in Fig. 7. The step from  $-3N$  to  $-5N$  occurs halfway through the horizontal line as the print head moves from left to right as indicated in Fig. 7. The white arrows indicate lines where the force is returned back to  $-3N$  before progressing into the next method. The lines were printed from bottom to top, starting with  $r'_{F,2}$  then  $r'_{F,5}$  and finally  $r_F$  which shows the performance of the LQR. The slight overshoot in  $F_{QP,2}$  that can be seen in the middle plot of Fig. 6 is not evident in Fig. 7 and does not seem to compromise the print quality.

Metric	LQR	LQR+QP		Improvement	
		$N_h = 2$	$N_h = 5$	$N_h = 2$	$N_h = 5$
RMSE (N)	0.278	0.173	<b>0.168</b>	37.77 %	<b>39.57 %</b>
$t_{5\%}(s)$	0.135	<b>0.022</b>	0.039	<b>83.70 %</b>	71.11 %

Table 2. Experimental Performance Metrics

As the optimization problem is run offline there is no run-time computational overhead or concerns for real time implementation; rather the main effort lies in coordinating the extrusion reference with specific spatial positions along the print bed via G-code. Through analyzing captured

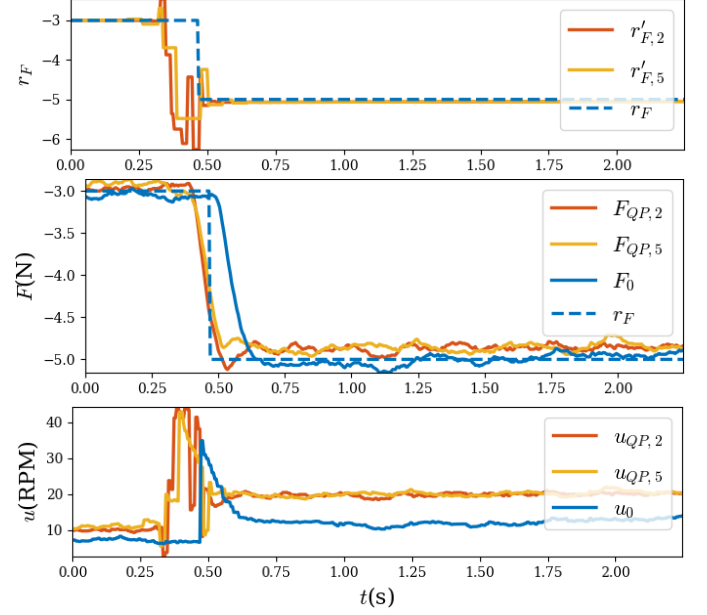


Fig. 6. Step Response on the Experimental Setup - Top: Force References - Middle: Force Measurements - Bottom: Extrusion RPM Input

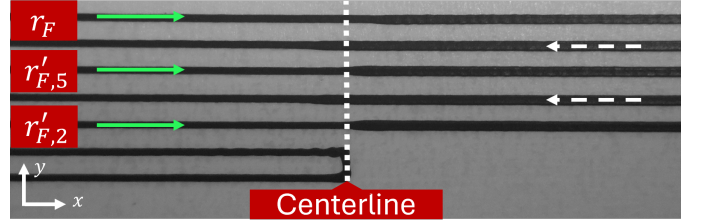


Fig. 7. Step Print Lines

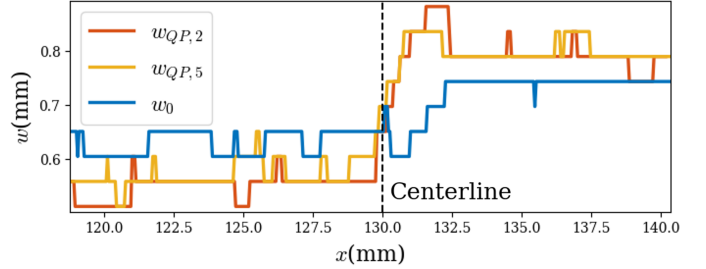


Fig. 8. Linewidths from Modified and Original References Extracted from Fig. 7

images of the print lines in 7, the respective linewidth  $w_0$  can be obtained in Fig. 8 upon applying LQR without modifying the reference force; the figure also presents the width obtained for different hold lengths ( $w_{QP,2}$  for  $N_h = 2$ , and  $w_{QP,5}$  for  $N_h = 5$ ). Evidently from Fig. 8 and Fig. 6, the LQR reacts slowly to the change in extrusion, leading to a gradual increase in linewidth. Experimentally, the shortcoming of the reactive LQR can be seen as the thickness of the extruded lines changing after the desired change-point at the center, in contrast to tracking the modified inputs which present an almost instantaneous change in width near the midpoint of the line.

#### 4. CONCLUSION

We present a formulation for the optimization of the force references to be tracked by FFF printers that compensates for the closed-loop performance of the printer. The formulation is implemented offline taking into consideration the behavior of the system in the presence of an LQR. Simulation results reveal performance improvement of up to 69.81% in RMSE. Experimentally, an improvement in the tracking error by 39.57% and response time by 83.7% is obtained, though model mismatch leads to the deviation of the experimental results from those obtained via simulation. Most importantly, there is no additional runtime computational overhead and the proposed QP can be solved very efficiently offline. Future work will investigate nonlinear extrusion behavior and nonlinear real-time control design. Future work also involves implementing the reference optimization online, in the presence of different types of controllers.

#### REFERENCES

- Bahrami, A., Watson, C., Tilbury, D., and Barton, K. (2025). Optimal feed-forward and iterative learning control framework for enhanced precision in extrusion-based additive manufacturing. In *International Manufacturing Science and Engineering Conference*, volume 89015, V001T01A012. American Society of Mechanical Engineers.
- Balta, E.C. and Altinkaynak, A. (2022). Numerical and experimental analysis of bead cross-sectional geometry in fused filament fabrication. *Rapid Prototyping Journal*, 28(10), 1882–1894. doi:10.1108/RPJ-09-2021-0255.
- Bellini, A., Güçeri, S., and Bertoldi, M. (2004). Liquefier dynamics in fused deposition. *Journal of Manufacturing Science and Engineering*, 126(2), 237–246. doi: 10.1115/1.1688377.
- Chessier, P., Post, B., Roschli, A., Carnal, C., Lind, R., Borish, M., and Love, L. (2019). Extrusion control for high quality printing on big area additive manufacturing (baam) systems. *Additive Manufacturing*, 28, 445–455.
- Fravolini, M.L., Rossi, A., Moretti, M., Senin, N., and Ferrante, F. (2025). Data-driven reference shaping for optimal fused filament fabrication. *Control Engineering Practice*, 164, 106511.
- Gao, J., Wu, P., Okwudire, C.E., and McGee, W. (2025). Using nonlinear lead filtering for real-time accurate extrusion control in large format additive manufacturing. *Additive Manufacturing*, 105005.
- Guidetti, X., Mingard, N., Cruz-Oliver, R., Nagel, Y., Rueppel, M., Rupenyan, A., Balta, E.C., and Lygeros, J. (2024a). Force controlled printing for material extrusion additive manufacturing. *Additive Manufacturing*, 89, 104297.
- Guidetti, X., Mukne, A., Rueppel, M., Nagel, Y., Balta, E.C., and Lygeros, J. (2024b). Data-driven extrusion force control tuning for 3d printing. In *2024 IEEE 20th International Conference on Automation Science and Engineering (CASE)*, 2262–2267. IEEE.
- Hornus, S., Kuipers, T., Devillers, O., Teillaud, M., Martínez, J., Glisse, M., Lazard, S., and Lefebvre, S. (2020). Variable-width contouring for additive manufacturing. *ACM Transactions on Graphics (TOG)*, 39(4), 131–1.
- Kolmanovsky, I., Garone, E., and Di Cairano, S. (2014). Reference and command governors: A tutorial on their theory and automotive applications. In *2014 American Control Conference*, 226–241. IEEE.
- Kuipers, T., Doubrovski, E.L., Wu, J., and Wang, C.C. (2020). A framework for adaptive width control of dense contour-parallel toolpaths in fused deposition modeling. *Computer-Aided Design*, 128, 102907.
- Moretti, M., Rossi, A., and Senin, N. (2021). In-process simulation of the extrusion to support optimisation and real-time monitoring in fused filament fabrication. *Additive Manufacturing*, 38, 101817.
- Moretti, M. and Rossi, A. (2023). Closed-loop filament feed control in fused filament fabrication. *3D Printing and Additive Manufacturing*, 10(3), 500–513. doi: 10.1089/3dp.2021.0236.
- Rabiee, M. and Moini, R. (2025). Extrusion under material uncertainty with pressure-based closed-loop feedback control in robotic concrete additive manufacturing. *Automation in Construction*, 180, 106494.
- Shi, T., Lu, B., Shen, T., Zhang, R., Shi, S., and Fu, G. (2018). Closed-loop control of variable width deposition in laser metal deposition. *The International Journal of Advanced Manufacturing Technology*, 97(9), 4167–4178.
- Singh, S., Singh, G., Prakash, C., and Ramakrishna, S. (2020). Current status and future directions of fused filament fabrication. *Journal of Manufacturing Processes*, 55, 288–306.
- Van Overschee, P. and De Moor, B. (1994). N4sid: Subspace algorithms for the identification of combined deterministic-stochastic systems. *Automatica*, 30(1), 75–93.
- Wu, P., Qian, C., and Okwudire, C.E. (2023). Modeling and feedforward control of filament advancement and retraction in material extrusion additive manufacturing. *Additive Manufacturing*, 78, 103850.
- Wu, P., Ramani, K.S., and Okwudire, C.E. (2021). Accurate linear and nonlinear model-based feedforward deposition control for material extrusion additive manufacturing. *Additive Manufacturing*, 48, 102389.
- Xia, C., Pan, Z., Zhang, S., Polden, J., Wang, L., Li, H., Xu, Y., and Chen, S. (2020). Model predictive control of layer width in wire arc additive manufacturing. *Journal of Manufacturing Processes*, 58, 179–186.
- Zhang, J., Wang, L., Lin, X., and Huang, W. (2024). Modeling of deposition morphology and characteristic dimensions in material extrusion additive manufacturing. *Additive Manufacturing*, 89, 104306.
- Zomorodi, H. and Landers, R.G. (2016). Extrusion based additive manufacturing using explicit model predictive control. In *2016 American Control Conference (ACC)*, 1747–1752. IEEE.